Spin-wave modes in permalloy/platinum wires and tuning of the mode damping by spin Hall current

Zheng Duan,* Carl T. Boone, Xiao Cheng, and Ilya N. Krivorotov
Department of Physics and Astronomy, University of California, Irvine, CA 92697, USA

Nathalie Reckers, Sven Stienen, and Michael Farle
Faculty of Physics and Center for Nanointegration (CeNIDE), Universität Duisburg-Essen, Lotharstr. 1, 47048 Duisburg, Germany

Jürgen Lindner
Institute of Ion Beam Physics and Materials Research, Helmholtz-Zentrum Dresden–Rossendorf, Bautzner Landstr. 400, 01328 Dresden, Germany

(Received 5 June 2014; revised manuscript received 8 July 2014; published 28 July 2014)

We report measurements of spectral properties of spin-wave modes in permalloy/platinum (Py/Pt) bilayer wires magnetized along two principal in-plane axes. We find that the spin torque arising from the spin Hall current in Pt can significantly reduce the spectral linewidth of the bulk and edge spin-wave modes of the wire magnetized perpendicular to its long axis. The linewidth reduction is strongest for the quasiuniform mode and weakest for the edge mode. Our work demonstrates the importance of extrinsic contributions to spin-wave damping for tuning of magnetization dynamics by spin Hall current.

DOI: 10.1103/PhysRevB.90.024427 PACS number(s): 76.50.+g, 75.30.Ds, 75.75.−c

I. INTRODUCTION

An electric charge current in a material with spin-orbit interaction can induce a pure spin current flowing perpendicular to the charge current—a phenomenon known as the spin Hall effect (SHE) [1–3]. If a ferromagnet (FM) is placed in close proximity to the nonmagnetic metal (NM), this pure spin current is injected into the FM from the NM and applies spin torque (ST) [4,5] to its magnetization [6–9]. Spin torque generated by SHE can act as negative magnetic damping proportional to the applied current density and thereby can induce a magnetic instability leading to either magnetization reversal [10] or magnetization auto-oscillations [11–14]. The manipulation of magnetization by ST arising from SHE is promising for applications in low-power nonvolatile ST memories [15–17] and microwave ST oscillators [18–24].

Spin torque from the pure spin current offers several key advantages for manipulation of magnetization over the conventional ST from spin-polarized electric charge current. First, the magnitude of spin current injected into the FM layer in a FM-NM bilayer can exceed that of the electric charge current in the system—a situation impossible for spin-polarized charge current [10]. Indeed, an electron participating in the charge current in the NM layer can scatter multiple times at the FM-NM interface and thereby can transfer more than a single quantum of angular momentum to the FM. Second, the use of FM/NM bilayer opens the possibility of scaling up ST devices without adverse effects arising from the Oersted field generated by the charge current. Indeed, the Oersted field in current-perpendicular-to-plane (CPP) spin valves (SV) used in conventional ST experiments is spatially inhomogeneous and, for a given current density, its maximum value scales linearly with the SV lateral dimensions. For a nanopillar SV as small as a few hundred nanometers in diameter, the Oersted field at the critical current density ranges from zero in the SV center to hundreds of Oersteds at the SV edge [25,26]. Such a strong spatially inhomogeneous magnetic field forces the magnetization into a vortex state, which restricts the studies of ST dynamics in the ground state of uniform magnetization to nanomagnets with lateral dimensions of ∼100 nm. In such small nanomagnets, the spin-wave spectrum degeneracy is lifted by the geometric confinement, and studies of the effect of ST on spin-wave interactions are complicated by the large energy gaps between the spin-wave modes [27,28]. In contrast, the Oersted field in SHE current-in-plane (CIP) structures is independent of the lateral dimensions of the structure, and the effect of ST on magnetization dynamics can be easily studied in micrometer-scale devices [29]. This opens the possibility of studying the effect of ST on multiple spin-wave modes and interactions between them in a wide variety of magnetic systems. Furthermore, ST from the pure spin current provides a unique opportunity to apply ST to ferromagnetic insulators due to its CIP geometry, which is impossible in conventional CPP SVs or magnetic tunnel junctions.

In this paper, we report the measurement of the spectral properties of spin-wave modes in micrometer-scale Py/Pt bilayer wires magnetized along two principal in-plane axes, as well as the tuning of the damping of these modes by the ST from SHE. Our measurements reveal that not all spin-wave modes are uniformly affected by ST from SHE and that the spectral linewidth of the quasiuniform mode is more susceptible to ST than that of other modes of the wire. We employ an electrically detected ferromagnetic resonance technique (FMR) [30,31] for measurements of spin-wave properties in Py/Pt wires. Figure 1(a) shows a scanning electron micrograph (SEM) of a typical device studied. A Py/Pt bilayer wire with four leads and shorted coplanar strips (CPS) in close proximity to the wire are defined on a GaAs substrate via e-beam lithography, evaporation, and liftoff. In our FMR measurements, a microwave current applied to the CPS generates a microwave magnetic field around the short, which excites spin waves in the Py wire. When the frequency of the microwave field coincides with the eigenfrequency of a

*justin.duan68@gmail.com

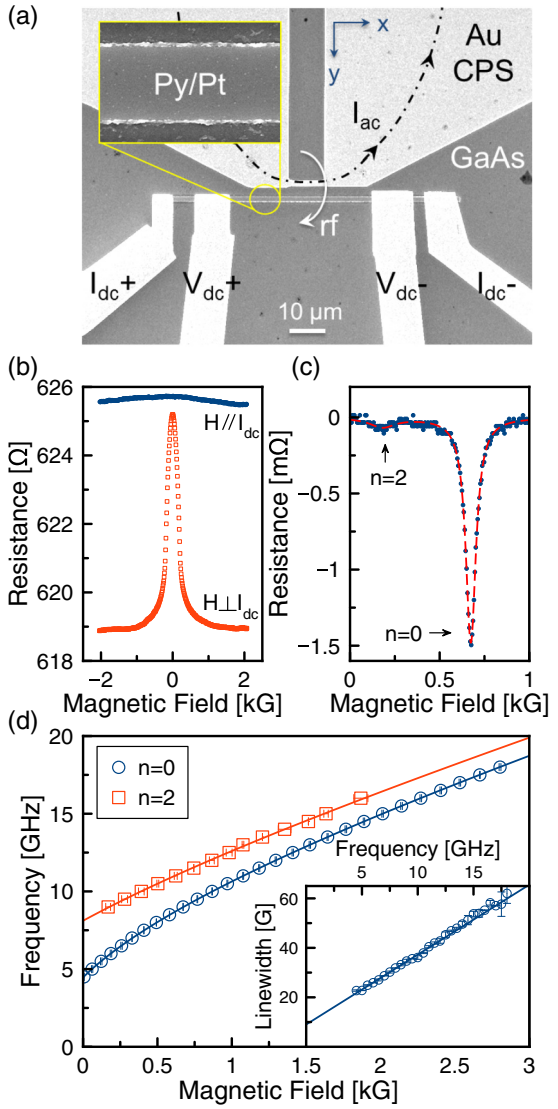

FIG. 1. (Color online) (a) SEM image of a 1.18-μm-wide Py (25 nm)/Pt (2 nm) wire device. The inset illustrates the degree of edge roughness of the wire. (b) Resistance versus magnetic field H for two in-plane directions of the field. (c) Resistively detected FMR spectrum measured at 9 GHz with H applied along the wire length. The dashed curve is a multipeak Lorentzian fit to the line shape. (d) Measured frequency versus H of $n = 2$ and $n = 0$ width modes for H applied along the wire. Lines are the best fit to Eq. (1). The inset shows the frequency dependence of the linewidth of the $n = 0$ width mode.

spin-wave mode in the wire, this mode is resonantly excited, leading to a change in the time-averaged wire resistance due to the anisotropic magnetoresistance (AMR) effect [Fig. 1(b)]. As shown in Fig. 1(c), we modulate the microwave field amplitude and employ lock-in measurements of the wire resistance as a function of external dc magnetic field (see Appendix A for details). The positive and negative peaks in such a measured, resistively detected FMR spectrum are signatures of the spin-wave eigenmodes in the Py wire. All measurements reported in this paper are performed at ambient temperature.

II. SPIN-WAVE MODES IN LONGITUDINALLY MAGNETIZED WIRES

Figure 1(c) shows a typical FMR spectrum measured at 9 GHz for a Py (25 nm)/Pt (2 nm), 1.18-μm-wide wire, with the external magnetic field H applied along its length. Through comparison to analytical theory [32] and micromagnetic simulations discussed below, the two spin-wave resonances observed at 179 and 674 G can be identified as $n = 2$ and $n = 0$ width modes [28], where n corresponds to the number of nodes in the spin-wave amplitude profile along the wire width direction. We apply a multipeak Lorentz function to fit the FMR spectra and obtain the resonance field and the linewidth (half width at half maximum) of each mode as a function of frequency, as shown in Fig. 1(d).

We find that the frequency versus field data in Fig. 1(d) are well described by the equation derived in Ref. [32] for magnetostatic width modes of thin-film strips

$$f_n = \frac{\gamma}{2\pi}\left[(H + N_n M_s)\left(H + (4\pi - N_n)M_s\right)\right]^{1/2}, \quad (1)$$

where f_n is the resonance frequency of the nth mode, $\gamma/2\pi = 2.92$ MHz/Oe is the gyromagnetic ratio, H is the external dc field, N_n represents the mode-specific dynamic demagnetizing factor ($N_n^x + N_n^y + N_n^z = 4\pi$) [32], and M_s is the saturation magnetization of the Py wire.

In our analysis, N_n and M_s are treated as fitting parameters. The best fit to the data shown in Fig. 1(d) yields $M_s = 790 \pm 0.5$ emu/cm^3 and $N_0 = 0.306 \pm 0.001$ for $n = 0$ mode, and $M_s = 788 \pm 7.6$ emu/cm^3 and $N_2 = 1.08 \pm 0.04$ for $n = 2$ mode. The saturation magnetization given by the fit is typical for Py thin films. In the approximation of pure dipolar pinning of the magnetization at the wire edges, the dynamic demagnetizing factors satisfy the following eigenvalue equation [33]:

$$(N_n - 4\pi)\boldsymbol{m_n}(y) = \int_{-w/2}^{w/2} dy' \frac{2}{t_{\mathrm{Py}}} \ln\left[\frac{(y-y')^2}{(y-y')^2 + t_{\mathrm{Py}}^2}\right] \boldsymbol{m_n}(y'), \quad (2)$$

where w is the width of the wire, t_{Py} is the thickness of the Py layer, $\boldsymbol{m_n}(y)$ is the amplitude of dynamic magnetization along the wire width. Using this expression, we calculate the expected values of the demagnetizing factors for $n = 0,1,2$ modes: $N_0 = 0.336$, $N_1 = 0.736$, and $N_2 = 1.14$. Comparison of the measured and calculated dynamic demagnetizing factors indicates that $n = 0,2$ modes are detected in the experiment. The odd symmetry modes (e.g., $n = 1$) are not excited due to spatial uniformity of the microwave field within the wire volume (approximately 17% variation in the field magnitude across the wire width), which results in weak coupling of the odd-symmetry modes to the microwave driving field.

The inset of Fig. 1(d) shows variation of the quasiuniform ($n = 0$) mode linewidth with frequency. The slope of the linear fit gives the effective damping of the mode: $\alpha_0 = \gamma/2\pi(d\Delta H/df) = 0.0082 \pm 0.0001$, a value similar to that of Py thin films. The linewidth does not extrapolate to zero at zero frequency, which can arise either from two-magnon scattering allowed for magnetic field applied parallel to the wire or from inhomogeneous broadening [28,34].

III. SPIN-WAVE MODES IN TRANSVERSELY MAGNETIZED WIRES

For a magnetic field applied in the sample plane perpendicular to the wire, multiple spin-wave modes are observed in the FMR spectrum, as shown in Fig. 2(a). Above a certain bulk saturation field $H_b = 210$ G, the magnetization of the wire becomes aligned with the applied field everywhere except near the wire edges. For $H > H_b$, several closely spaced resonances seen in the spectrum can be identified as bulk spin-wave modes, whose amplitude is significant in the interior of the wire and is small near the wire edges [32,35]. At yet higher fields above the edge saturation field $H > H_e = 1200$ G, the magnetization of the wire becomes completely saturated, and a saturated edge spin-wave mode, whose amplitude is maximum at the wire edges [36,37], gives rise to a positive peak in the FMR spectrum. The bulk and edge saturation fields can be clearly identified as local minima in the dependence of the mode frequency on the field, shown in the top panel of Fig. 2(b) [36].

The experimentally observed dependence of the mode frequency on magnetic field is in good agreement with our Object Oriented MicroMagnetic Framework (OOMMF) micromagnetic simulations [38], shown in the bottom panel of Fig. 2(b). These simulations allow us to identify the modes observed in the experiment and to determine the spatial profiles of their amplitudes. The highest frequency mode at $H > H_b$ is identified as the quasiuniform mode, whose amplitude monotonically decays from a maximum in the middle of the wire to a small value near the wire edges. Several modes with slightly lower frequencies are identified as bulk modes with nodes in the wire width direction [32]. The lowest frequency mode is identified as the edge mode, the amplitude of which is nearly zero in the middle of the wire and reaches maximum at the wire edges [36]. The main difference between the measured and the simulated dependences of the mode frequency on field is the value of the edge saturation field H_e (1200 G in the experiment versus 2100 G in the simulation). This difference mainly arises from the wire edge roughness shown in Fig. 1(a), which is known to reduce the edge saturation field compared to that of a wire with perfectly flat edges assumed in the simulation [36,39].

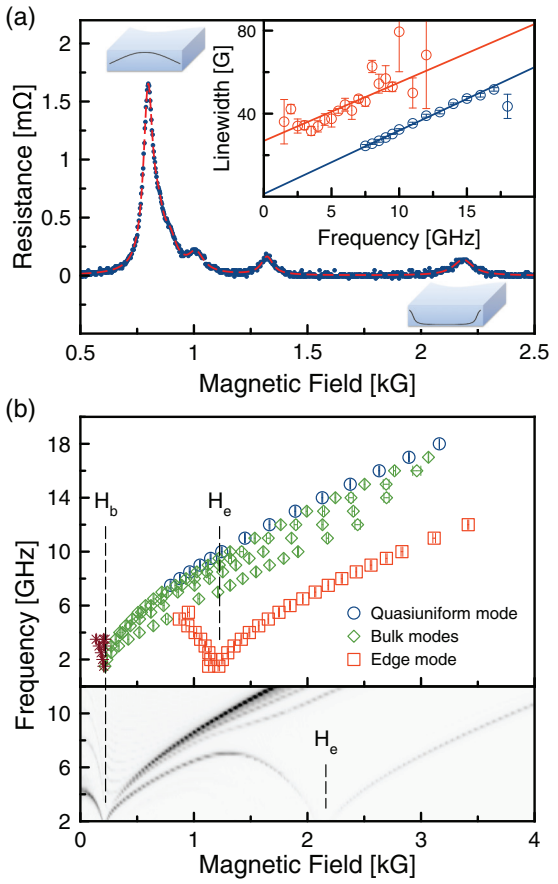

FIG. 2. (Color online) (a) Resistively detected FMR spectrum measured at 7.5 GHz, with H applied in the sample plane perpendicular to the wire. The dashed curve is a multipeak Lorentzian fit to the line shape. The schematic amplitude profiles along the wire width for the quasiuniform and edge modes are shown. Inset: spectral linewidth of the quasiuniform and edge modes versus frequency. (b) Measured (top) and simulated (bottom) dependence of spin-wave modes frequency on H.

The linewidths of the quasiuniform mode and the edge mode are plotted versus frequency in the inset of Fig. 2(a). Linear fits to these data yield the effective damping parameters $\alpha_0 = 0.0089 \pm 0.0002$ for the former and $\alpha_e = 0.0083 \pm 0.0016$ for the latter. Both values are close to that of Py thin films. For the edge mode, the linear fit crosses the vertical axis far from the origin. This extrinsic contribution to the linewidth may result from inhomogeneous broadening induced by the nanowire edge roughness, which is expected to have large impact on the edge mode frequency and linewidth [36]. For the quasiuniform mode, the linear fit passes near the origin. This may be explained by the smallness of the quasiuniform mode amplitude at the wire edges, where magnetic inhomogeneities, such as edge roughness, are expected to be large.

IV. TUNING THE DAMPING OF SPIN-WAVE MODES BY SPIN HALL CURRENT

Next, we study the effect of dc on spin-wave modes in the Py wire with the field applied in the sample plane perpendicular to the wire. In this geometry, the spin polarization of the pure spin current generated in the Pt layer by SHE is collinear with the magnetization of the Py layer for $H > H_e$. This collinear spin current injected into the Py layer applies ST to its magnetization and, depending on the current polarity, acts as either positive or negative magnetic damping that can modify the linewidth of spin-wave resonances in the FMR spectrum [6]. The spectral linewidth of the quasiuniform mode $\Delta H_0 (I_{dc})$ at direct current I_{dc} in the presence of only Gilbert damping and spin current contribution can be approximated by the thin-film expression [40]:

$$\Delta H_0 (I_{dc}) = \frac{2\pi f_0}{\gamma} \alpha_0 (I_{dc}) = \frac{2\pi f_0}{\gamma} \left(\alpha_G + \frac{1}{(H_0 + 2\pi M_s)} \frac{\hbar J_s}{4e M_s t_{Py}} \right), \quad (3)$$

where f_0 and H_0 are the resonance frequency and resonance field of the quasiuniform mode, respectively, $\alpha_0 (I_{dc})$ is the effective damping of the quasiuniform mode at I_{dc}, α_G is the Gilbert damping parameter, J_s is the spin current density

(in units of charge current density) injected into Py, $\hbar$ and e are the reduced Planck constant and electron charge, respectively. Such an approximation is justified for the quasiuniform mode because this mode shows no extrinsic contributions to damping [see the inset of Fig. 2(a)] and because the width of the wire is much greater than its thickness (see Appendix B for details).

The magnitude of J_s significantly decreases when the thickness of the Pt layer is reduced to values below ∼5 nm [40,41]; thus, we choose wires with a thicker Pt layer: Py (19 nm)/Pt (5 nm) for studies of the effect of spin current on spin-wave damping. Figure 3(a) shows FMR spectra for a 0.61 μm-wide Py (19 nm)/Pt (5 nm) wire measured at an excitation frequency of 8.5 GHz in the presence of positive and negative bias current $I_{dc} = \pm 6.12$ mA applied to the wire. First, we note that the

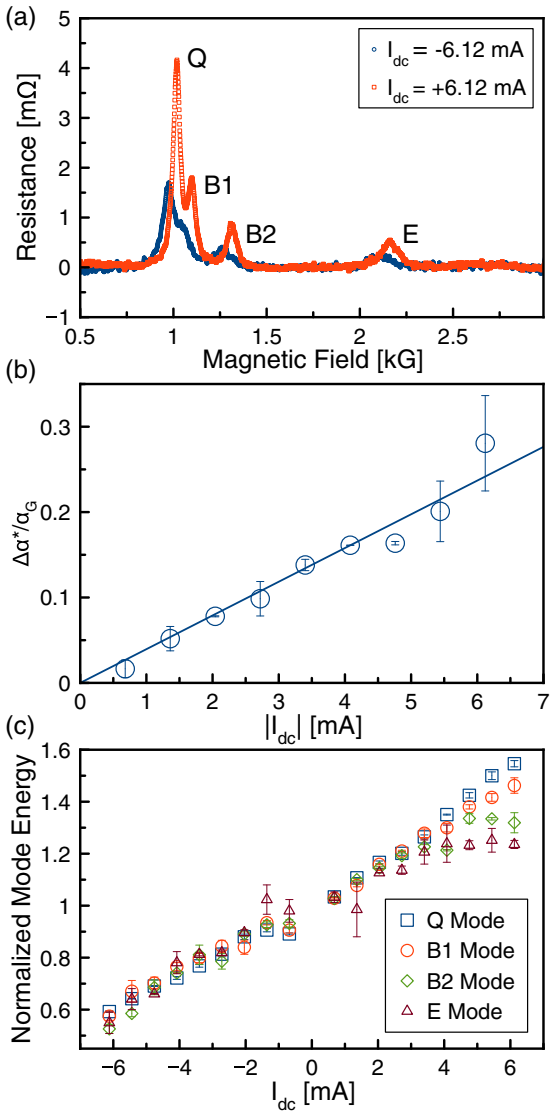

FIG. 3. (Color online) (a) FMR spectra of a Py (19 nm)/Pt (5 nm) 0.61-μm-wide wire measured at 8.5 GHz for $I_{dc} = \pm 6.12$ mA. The field is applied in the sample plane perpendicular to the wire. (b) Fractional change of the effective damping induced by spin Hall torque for the quasiuniform mode versus dc. The line is a linear fit. (c) Normalized energy stored in four spin-wave modes at their resonance fields versus current: Q, quasiuniform mode; B1, first bulk mode; B2, second bulk mode; E, edge mode.

current-induced frequency shift for all modes arises from the Oersted field (3. G/mA) generated by the current flowing in the Pt layer. Second, the spectral linewidth of all spin-wave resonances is significantly modified by the current. At positive currents, the linewidth decreases, and the amplitude increases with increasing current for all modes, while the opposite trend is observed for negative currents. Because Ohmic heating equally affects both current polarities, we calculate the difference of the effective damping parameter measured at positive and negative currents $\alpha_0(+I_{dc}) - \alpha_0(-I_{dc})$ in order to determine the effect of spin Hall torque on the damping of the quasiuniform mode. For this mode, the fractional change in the effective damping due to spin Hall current $\Delta\alpha^*/\alpha_G = |\alpha_0(+I_{dc}) - \alpha_0(-I_{dc})|/2\alpha_G$ is plotted versus the charge current magnitude in Fig. 3(b). This figure illustrates that the effective damping of the quasiuniform mode is linear in current, as expected from Eq. (3) and that a reduction of damping by ∼25% due to SHE can be achieved at the largest current densities used in the experiment. The ratio of the spin current density J_s to the charge current density J in Pt can be calculated from the slope of the linear fit in Fig. 3(b) and Eq. (3):

$$\frac{J_s}{J} = \frac{\Delta\alpha^* (H_0 + 2\pi M_s) 4eM_s t_{Py}}{\hbar J} = 0.066 \pm 0.003, \quad (4)$$

where we use $\alpha_G = 0.0077$, which is determined from the FMR data with the magnetic field applied parallel to the wire similar to those shown in Fig. 1(c). We also use the following resistivities to determine the current density J in the Pt layer: $\rho_{Pt} = 21.9\ \mu\Omega\cdot$cm, $\rho_{Py} = 65.2\ \mu\Omega\cdot$cm (see Appendix C).

To quantify the effect of spin current on different modes shown in Fig. 3(a), we calculate the normalized mode energy stored in each mode at the corresponding resonance field $E_n^*(I_{dc}) = E_n(I_{dc})/E_n(I_{dc} = 0)$ and plot it as a function of the current bias in Fig. 3(c). In the limit of a small precession angle, $E_n(I_{dc})$ is directly determined from the FMR peak amplitude A_n of the nth spin-wave mode [42]:

$$E_n(I_{dc}) \propto \frac{\theta_n^2}{2} \propto \frac{A_n}{I_{dc} R_{AMR}}, \quad (5)$$

where θ_n is the maximum in-plane precession angle of the nth mode and R_{AMR} is the difference in resistance of the wire magnetized along its length and along its width (full AMR).

In the absence of extrinsic contributions to the spectral linewidth (valid for the quasiuniform mode), we expect the following dependence of the mode energy on current density:

$$E_0^*(I_{dc}) = \frac{E_0(I_{dc})}{E_0(I_{dc} = 0)} \propto \frac{\alpha_0^2(I_{dc} = 0)}{\alpha_0^2(I_{dc})} = \frac{1}{(1 - J/J_0)^2}, \quad (6)$$

where α_0 and J_0 are the effective damping and critical current of the quasiuniform mode. Equation (6) predicts a squared hyperbolic dependence of the normalized mode energy on current but the measured E_0^* does not show the expected positive curvature. We attribute this to Ohmic heating, which enhances the spin-wave linewidth for both current polarities [29]. Indeed, the effect of Ohmic heating is clearly seen from a decrease of the wire's AMR and saturation magnetization with increasing current (see Appendix D). The remaining modes observed show even greater deviation from the squared hyperbolic dependence on current. We attribute the difference in the deviation to the inhomogeneous broadening

of the spectral linewidths of these modes (described in more detail in Appendix B), which is unlikely to be affected by the spin current. Hence, modes (e.g., edge mode) with larger inhomogeneous broadening appear less susceptible to the spin current, and the observed change in the mode energy becomes smaller. For positive currents, $E_n^*(I_{\rm dc})$ of the two high-field modes (B2 and E) approaches saturation at large current densities. This behavior, opposite to the predicated divergence at the critical current, suggests that Ohmic heating in the system under study precludes it from reaching the state of magnetization self-oscillation. Thus, a wire with a significantly thinner Py layer and thereby lower critical current is needed for the excitation of ST-driven oscillations by SHE.

The geometric quantization of the spin-wave spectrum in the wire allows us to study the effect of ST from SHE on individual spin-wave modes. The data in Fig. 3(c) reveal that the linewidth of the quasiuniform mode is more susceptible to ST from pure spin current than that of the other modes. We note that the quasiuniform mode is the only mode that shows no extrinsic contributions to damping [34], as illustrated in the inset of Fig. 2(a), and thus its spectral linewidth is expected to be more susceptible to spin current (see Appendix B). Additionally, the vertical component of spin current density J_s near the nanowire edge is expected to be weaker than that near the wire center for two reasons: (i) smaller charge current density near the edges due to enhanced electron scattering at the wire edge and (ii) rotation of the spin current polarization to the out-of-plane direction near the wire edge [3]. This should reduce susceptibility of the edge mode to spin Hall current. Thus, we conclude that extrinsic contributions to damping generally caused by spatial inhomogeneity of magnetization and magnetic anisotropy, as well as spatial nonuniformity of the spin Hall current, strongly influence the dependence of spin-wave mode linewidth on spin Hall currents.

V. SUMMARY

In summary, we used resistively detected FMR to study spectral properties of spin-wave modes in Py/Pt bilayer wires. We demonstrated that ST arising from pure spin current in the Pt layer can efficiently tune the spectral linewidth of these spin-wave modes. The spectral linewidths of these modes are not uniformly affected by the current, and the quasiuniform mode is the mode most susceptible to spin current. We explain this behavior by inhomogeneous contributions to the linewidth of the bulk and edge spin-wave modes, as well as by spatial nonuniformity of the spin current within the wire. Our data also suggest that Ohmic heating can increase damping of all spin-wave modes—an effect that can become stronger than reduction of damping by the spin Hall current at high current densities.

ACKNOWLEDGMENTS

This work was supported by Sonderforschungsbereich (SFB) 491, a project under Deutsche Forschungsgemeinschaft (DFG), by National Science Foundation (NSF) Grants No. DMR-1210850, No. DMR-0748810, No. DMR-1124601, No. ECCS-1002358, and by the Function Accelerated nanoMaterial Engineering (FAME) Center, one of six centers of Semiconductor Technology Advanced Research Network (STARnet), a Semiconductor Research Corporation program sponsored by Microelectronics Advanced Research Corporation (MARCO) and Defense Advanced Research Projects Agency (DARPA). Funding by the DFG/NSF in the framework of the "Materials World Network" program is also acknowledged.

APPENDIX A: FMR BACKGROUND SUBTRACTION

The raw voltage signal measured by our resistively detected FMR setup consists of two components: one arises from bolometric heating of the Py/Pt wire by the microwave drive, and the other component is due to magnetization precession that affects the voltage signal via the AMR effect. The bolometric heating signal V_b is always present because the wire is periodically heated by the amplitude-modulated microwave field, which generates eddy currents in the wire and thereby induces periodic variation of the wire temperature and resistance at the modulation frequency. The AMR signal can be further split into two parts. One part arises from variation of the time-averaged resistance of the sample in response to the microwave drive (photoresistance [42]). This signal V_{PR} is proportional to the dc applied to the wire. The other part of the signal is photovoltage V_{PV} [42–44], a rectified signal arising from mixing of the nanowire resistance oscillations at the microwave drive frequency and the microwave eddy currents in the wire. The photovoltage signal V_{PV} increases with increasing microwave drive amplitude and is nearly independent of the dc bias. Hence, the net voltage signal [45] detected by our lock-in amplifier at the modulation frequency of the microwave drive is

$$V = V_b + V_{PR} + V_{PV} = I_{\rm dc}\delta R_b + I_{\rm dc}\delta R_{\rm dc} + I_{ac}\delta R_{ac}\cos\theta, \tag{A1}$$

where $I_{\rm dc}$ is the direct bias current applied to the wire, I_{ac} is the microwave eddy current amplitude in the wire, δR_b is the amplitude of the wire resistance oscillations due to the bolometric heating, $\delta R_{\rm dc}$ is the amplitude of the time-averaged resistance oscillations at the modulation frequency arising from the AMR effect, δR_{ac} is the amplitude of the microwave resistance oscillations arising from the AMR effect, and θ is the phase shift between the microwave eddy current in the wire and the microwave resistance oscillations.

Because bolometric heating V_b is independent on the bias magnetic field H, it appears as a field-independent background in a field-swept FMR spectrum $V(H)$; thus, it can be simply removed by subtracting a constant from the measured spectrum. The photovoltage and photoresistance signals arising from the excitation of spin-wave resonances in the wire appear in the FMR spectra as peaks with different symmetries. The photoresistance signal gives rise to a symmetric Lorentzian peak in the spectrum, while photovoltage generally gives rise to a peak that is a sum of symmetric and antisymmetric Lorentzians [42]:

$$I_{\rm dc}\delta R_{\rm dc} = U_{PR}\frac{\Delta H^2}{(H-H_0)^2+\Delta H^2}, \tag{A2a}$$

$$I_{ac}\delta R_{ac}\cos\theta = U_{PV}^{S}\frac{\Delta H^2}{(H-H_0)^2+\Delta H^2} + U_{PV}^{A}\frac{(H-H_0)\,\Delta H}{(H-H_0)^2+\Delta H^2}. \tag{A2b}$$

A nonzero photovoltage greatly complicates the FMR data analysis, especially when several closely spaced modes are present in the spectrum. Consequently, we only employ experimental geometries, in which the photovoltage contribution is either minimized or completely eliminated. The photovoltage signal is completely removed when the nanowire is magnetized exactly along its length. In this geometry, the wire resistance oscillates at twice the frequency of the magnetization (and the eddy current) oscillations, thus the mixing voltage (photovoltage) is zero. However, the photovoltage signal generally cannot be completely eliminated for the magnetic field applied along the wire width. In this geometry, magnetization at the wire edges makes a nonzero angle with the applied field direction for applied fields below the edge saturation field H_e. Hence, the photovoltage signal component is always present for $H < H_e$. In order to eliminate the photovoltage component in this case, we measure FMR spectra at opposite dc polarities and subtract the spectra from each other. This difference of two FMR spectra does not contain a photovoltage signal component. Indeed, the net signals measured at two current polarities are

$$V(+I_{\rm dc}) = (+I_{\rm dc})\delta R_b + (+I_{\rm dc})\delta R_{\rm dc} + I_{ac}\delta R_{ac}\cos\theta, \quad \text{(A3a)}$$

$$V(-I_{\rm dc}) = (-I_{\rm dc})\delta R_b + (-I_{\rm dc})\delta R_{\rm dc} + I_{ac}\delta R_{ac}\cos\theta. \quad \text{(A3b)}$$

The photoresistance and photovoltage terms are, thus, calculated from the difference and the sum of the two FMR curves (see Fig. 4):

$$V_b + V_{PR} = \frac{V(+I_{\rm dc}) - V(-I_{\rm dc})}{2}, \quad \text{(A4a)}$$

$$V_{PV} = \frac{V(+I_{\rm dc}) + V(-I_{\rm dc})}{2}. \quad \text{(A4b)}$$

We note that the method of Eqs. (A4a) and (A4b) works well only for relatively low values of the dc because, at large bias current values, opposite current polarities (i) introduce significant shifts of the spectral lines in opposite field directions due to the current-induced Oersted field and (ii) noticeably and asymmetrically modify the spectral linewidths of the photoresistance signal via the SHE. To solve this problem, we use a different procedure for subtraction of the photovoltage component of the signal at large values of the direct bias current. This method relies on independence of the photovoltage signal on dc bias. In this method, we first measure the photovoltage at zero current bias, at which the FMR signal has zero photoresistance component. Then, we subtract the zero-bias FMR curve from a finite bias FMR curve to obtain a pure photoresistance signal at the finite current bias. In this subtraction procedure, we shift the zero-bias FMR curve along the magnetic field axis to compensate for the Oersted field acting on the Py layer from current in the Pt layer. This Oersted field is easily calculated given the values of the thickness and resistivity of the Pt and Py layers. The main conceptual drawback of this method is that it neglects the effects of Ohmic heating and spin Hall current on the photovoltage signal. However, we find the errors introduced by neglecting these effects to be insignificant in practice. Indeed, the magnitude of the photoresistance signal increases linearly with increasing dc bias, while the photovoltage signal magnitude is nearly independent on the bias current. Thus, although the absolute effect of the current on the photovoltage signal increases with increasing current, the relative contribution of the photovoltage to the overall signal decreases. We find that, in practice, the current-induced effect on the photovoltage introduces insignificant errors to the pure photoresistance signal obtained from the raw FMR data via this procedure.

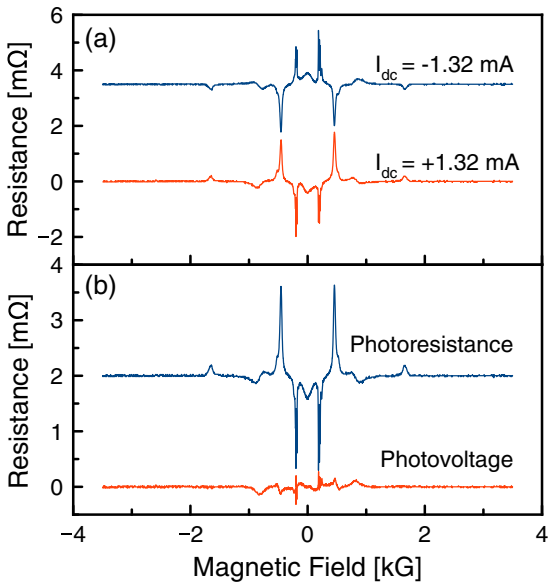

FIG. 4. (Color online) FMR spectra $V(H)/I_{\rm dc}$ measured at 5 GHz for a 1.18-μm-wide Py (25 nm)/Pt (2 nm) wire magnetized along its width. The field-independent bolometric heating background is removed, and the curves are vertically offset for clarity. (a) FMR signals measured at $I_{\rm dc} = \pm$ 1.32 mA. (b) The photoresistance and the photovoltage components of the signal calculated from the data in (a) according to Eqs. (A4a) and (A4b).

APPENDIX B: EXTRINSIC LINE BROADENING AND THE LINEWIDTH DEPENDENCE ON SPIN CURRENT

In the main text, we argue that extrinsic contributions to the linewidth of a spin-wave mode, such as inhomogeneous broadening, can weaken the dependence of the spectral linewidth of a mode on spin current. This can be illustrated by an example of inhomogeneous broadening of a mode due to Gaussian distribution of the mode resonance fields in different locations along the nanowire (e.g., induced by spatial fluctuations of the wire width). In this case, the spectral line of the mode is a convolution of the intrinsic Lorentzian line with the Gaussian distribution of the resonance fields:

$$\int_{-\infty}^{+\infty} e^{-\left(\frac{H_r - H_{r0}}{\sqrt{2}\sigma}\right)^2} \frac{1}{(H - H_r)^2 + \delta H^2} dH_r, \quad \text{(B1)}$$

where H_r is the resonance field, H_{r0} is the mean, σ is the width of the resonance field distribution, and δH is the intrinsic linewidth of the mode. To illustrate the effect of inhomogeneous line broadening on the linewidth tuning by spin current, we assume linear dependence of δH on current [as described by Eq. (3) of the main text] and plot the dependence of spectral linewidth and normalized mode energy on current

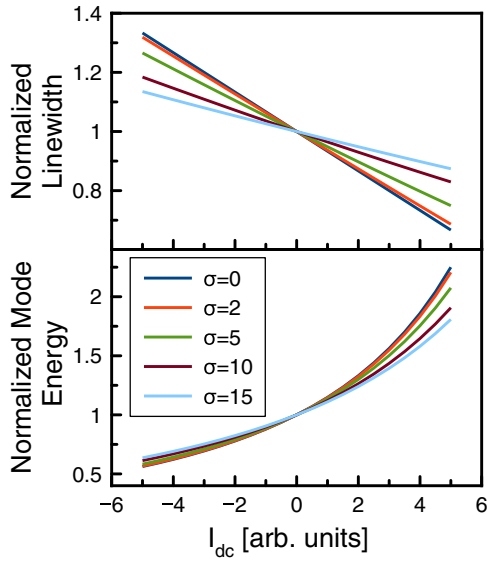

FIG. 5. (Color online) Predicted normalized linewidth (top) and normalized mode energy (bottom) at the absence of Ohmic heating as functions of I_{dc} for several values of σ, $H_{r0} = 500$, and $\delta H(I_{dc} = 0) = 15$.

for $\sigma = 0$ and $\sigma > 0$ in Fig. 5. This figure clearly shows that stronger inhomogeneous broadening reduces the dependence of linewidth and mode energy on current.

APPENDIX C: MEASUREMENT OF PT AND PY LAYER RESISTIVITY

In order to determine the current density J in Pt, we assume that Py and Pt layers form a parallel resistor circuit, hence,

$$J = \frac{I_{dc}}{w t_{Pt}} \frac{\rho_{Py}/t_{Py}}{\rho_{Py}/t_{Py} + \rho_{Pt}/t_{Pt}}, \tag{C1}$$

where w is the width of the wire, t_{Py} and t_{Pt} are the thicknesses of the Py and Pt layers, respectively, ρ_{Py} and ρ_{Pt}

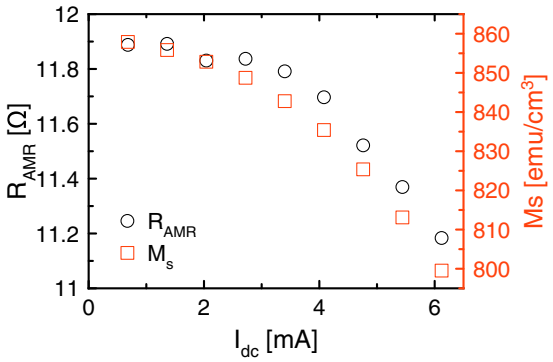

FIG. 6. (Color online) Dependence of the full AMR resistance R_{AMR} and saturation magnetization M_s on dc I_{dc}.

are the corresponding resistivities that are determined from measurements of resistance of the Py/Pt bilayer wires with different thicknesses of the layers:

$$\frac{1}{R_{wire}} = \left(\frac{t_{Pt}}{\rho_{Pt}} + \frac{t_{Py}}{\rho_{Py}}\right)\frac{w}{l}, \tag{C2}$$

where R_{wire} is the bilayer wire resistance and l is the length of the wire. By changing the layer thicknesses and measuring the bilayer wire resistance, ρ_{Pt} and ρ_{Py} are independently determined ($\rho_{Pt} = 21.9\ \mu\Omega\cdot$cm, $\rho_{Py} = 65.2\ \mu\Omega\cdot$cm).

APPENDIX D: DEPENDENCE OF AMR AND SATURATION MAGNETIZATION ON CURRENT BIAS

In the calculation of the ratio between the spin and charge current density J_s/J and the mode energy, due to the Ohmic heating, the current bias dependence of the full AMR R_{AMR} and the wire saturation magnetization M_s (shown in Fig. 6) must be taken into account. $R_{AMR}(I_{dc})$ is measured directly, while $M_s(I_{dc})$ is determined from fitting Eq. (1) of the main text to FMR data collected at nonzero I_{dc} with the magnetic field applied along the wire length.

[1] M. I. Dyakonov and V. I. Perel, Sov. Phys. JETP Lett. **13**, 467 (1971).
[2] J. E. Hirsch, Phys. Rev. Lett. **83**, 1834 (1999).
[3] Y. K. Kato, R. C. Myers, A. C. Gossard, and D. D. Awschalom, Science **306**, 1910 (2004).
[4] J. C. Slonczewski, J. Magn. Magn. Mater. **159**, L1 (1996).
[5] L. Berger, Phys. Rev. B **54**, 9353 (1996).
[6] K. Ando, S. Takahashi, K. Harii, K. Sasage, J. Ieda, S. Maekawa, and E. Saitoh, Phys. Rev. Lett. **101**, 036601 (2008).
[7] V. E. Demidov, S. Urazhdin, E. R. J. Edwards, and S. O. Demokritov, Appl. Phys. Lett. **99**, 172501 (2011).
[8] Z. Wang, Y. Sun, M. Wu, V. Tiberkevich, and A. Slavin, Phys. Rev. Lett. **107**, 146602 (2011).
[9] Z. Wang, Y. Sun, Y.-Y. Song, M. Wu, H. Schultheiß, J. E. Pearson, and A. Hoffmann, Appl. Phys. Lett. **99**, 162511 (2011).
[10] L. Liu, C.-F. Pai, Y. Li, H. W. Tseng, D. C. Ralph, and R. A. Buhrman, Science **336**, 555 (2012).
[11] V. E. Demidov, S. Urazhdin, H. Ulrichs, V. Tiberkevich, A. Slavin, D. Baither, G. Schmitz, and S. O. Demokritov, Nat. Mater. **11**, 1028 (2012).
[12] R. H. Liu, W. L. Lim, and S. Urazhdin, Phys. Rev. Lett. **110**, 147601 (2013).
[13] L. Liu, C.-F. Pai, D. C. Ralph, and R. A. Buhrman, Phys. Rev. Lett. **109**, 186602 (2012).
[14] H. Ulrichs, V. E. Demidov, S. O. Demokritov, W. L. Lim, J. Melander, N. Ebrahim-Zadeh, and S. Urazhdin, Appl. Phys. Lett. **102**, 132402 (2013).
[15] J. A. Katine, F. J. Albert, R. A. Buhrman, E. B. Myers, and D. C. Ralph, Phys. Rev. Lett. **84**, 3149 (2000).

[16] B. Özyilmaz, A. D. Kent, D. Monsma, J. Z. Sun, M. J. Rooks, and R. H. Koch, Phys. Rev. Lett. **91**, 067203 (2003).
[17] S. Manipatruni, D. E. Nikonov, and I. A. Young, arXiv:1301.5374.
[18] S. I. Kiselev, J. C. Sankey, I. N. Krivorotov, N. C. Emley, R. J. Schoelkopf, R. A. Buhrman, and D. C. Ralph, Nature (London) **425**, 380 (2003).
[19] W. H. Rippard, M. R. Pufall, S. Kaka, S. E. Russek, and T. J. Silva, Phys. Rev. Lett. **92**, 027201 (2004).
[20] I. N. Krivorotov, N. C. Emley, J. C. Sankey, S. I. Kiselev, D. C. Ralph, and R. A. Buhrman, Science **307**, 228 (2005).
[21] D. Houssameddine, U. Ebels, B. Delaet, B. Rodmacq, I. Firastrau, F. Ponthenier, M. Brunet, C. Thirion, J.-P. Michel, L. Prejbeanu-Buda, M.-C. Cyrille, O. Redon, and B. Dieny, Nat. Mater. **6**, 447 (2007).
[22] A. Ruotolo, V. Cros, B. Georges, A. Dussaux, J. Grollier, C. Deranlot, R. Guillemet, K. Bouzehouane, S. Fusil, and A. Fert, Nat. Nanotechnol. **4**, 528 (2009).
[23] A. M. Deac, A. Fukushima, H. Kubota, H. Maehara, Y. Suzuki, S. Yuasa, Y. Nagamine, K. Tsunekawa, D. D. Djayaprawira, and N. Watanabe, Nat. Phys. **4**, 803 (2008).
[24] P. K. Muduli, Y. Pogoryelov, S. Bonetti, G. Consolo, F. Mancoff, and J. Akerman, Phys. Rev. B **81**, 140408(R) (2010).
[25] K. Bussman, G. A. Prinz, S. F. Cheng, and D. Wang, Appl. Phys. Lett. **75**, 2476 (1999).
[26] F. J. Albert, J. A. Katine, R. A. Buhrman, and D. C. Ralph, Appl. Phys. Lett. **77**, 3809 (2000).
[27] J. C. Sankey, P. M. Braganca, A. G. F. Garcia, I. N. Krivorotov, R. A. Buhrman, and D. C. Ralph, Phys. Rev. Lett. **96**, 227601 (2006).
[28] C. T. Boone, J. A. Katine, J. R. Childress, V. Tiberkevich, A. Slavin, J. Zhu, X. Cheng, and I. N. Krivorotov, Phys. Rev. Lett. **103**, 167601 (2009).
[29] V. E. Demidov, S. Urazhdin, E. R. J. Edwards, M. D. Stiles, R. D. McMichael, and S. O. Demokritov, Phys. Rev. Lett. **107**, 107204 (2011).
[30] M. V. Costache, S. M. Watts, M. Sladkov, C. H. van der Wal, and B. J. van Wees, Appl. Phys. Lett. **89**, 232115 (2006).
[31] K. Ando, J. Ieda, K. Sasage, S. Takahashi, S. Maekawa, and E. Saitoh, Appl. Phys. Lett. **94**, 262505 (2009).
[32] C. Bayer, J. Jorzick, S. O. Demokritov, A. N. Slavin, K. Y. Guslienko, D. V. Berkov, N. L. Gorn, M. P. Kostylev, and B. Hillebrands, Top. Appl. Phys. **101**, 57 (2006).
[33] K. Y. Guslienko, S. O. Demokritov, B. Hillebrands, and A. N. Slavin, Phys. Rev. B **66**, 132402 (2002).
[34] R. Arias and D. L. Mills, Phys. Rev. B **60**, 7395 (1999).
[35] J. P. Park, P. Eames, D. M. Engebretson, J. Berezovsky, and P. A. Crowell, Phys. Rev. Lett. **89**, 277201 (2002).
[36] R. D. McMichael and B. B. Maranville, Phys. Rev. B **74**, 024424 (2006).
[37] M. Bailleul, D. Olligs, and C. Fermon, Phys. Rev. Lett. **91**, 137204 (2003).
[38] M. Donahue and D. Porter, OOMMF User's Guide, Version 1.0, Interagency Report NISTIR 6376 (National Institute of Standards and Technology, Gaithersburg, MD, 1999).
[39] R. P. Cowburn, D. K. Koltsov, A. O. Adeyeye, and M. E. Welland, J. Appl. Phys. **87**, 7067 (2000).
[40] L. Liu, T. Moriyama, D. C. Ralph, and R. A. Buhrman, Phys. Rev. Lett. **106**, 036601 (2011).
[41] Hans T. Nembach, Justin M. Shaw, Carl T. Boone, and T. J. Silva, Phys. Rev. Lett. **110**, 117201 (2013).
[42] N. Mecking, Y. S. Gui, and C.-M. Hu, Phys. Rev. B **76**, 224430 (2007).
[43] H. J. Juretschke, J. Appl. Phys. **31**, 1401 (1960).
[44] H. J. Juretschke, J. Appl. Phys. **34**, 1223 (1963).
[45] The voltages measured refer to the rms value of the first harmonic of each signal component at the modulation frequency.